



## **Octreotide used for Probing the Type-II' $\beta$ -turn CD and Raman Markers**

Belén Hernández,<sup>a♦</sup> Yves-Marie Coïc,<sup>b♦</sup> Sergei Kruglik,<sup>c</sup> Claude Carelli,<sup>d</sup> Régis Cohen,<sup>e</sup>  
Mahmoud Ghomi<sup>a\*</sup>

<sup>a</sup>Université Paris 13, Sorbonne Paris Cité, Groupe de Biophysique Moléculaire, UFR Santé-Médecine-Biologie Humaine, 74 rue Marcel Cachin, 93017 Bobigny cedex, France

<sup>b</sup>Institut Pasteur, Unité de Chimie des Biomolécules, UMR 3523, 28 rue du Docteur Roux, 75724 Paris Cedex 15, France

<sup>c</sup>Laboratoire Jean Perrin, FRE 3231, Université Pierre et Marie Curie (Paris 6), Case courrier 138, 75252 Paris cedex 05, France

<sup>d</sup>Université Paris Descartes, Sorbonne Paris Cité, Synthèse et Structure de Molécules d'Intérêt Pharmacologique, UMR 8638, Faculté des Sciences Pharmaceutiques et Biologiques, 4 Avenue de l'Observatoire, 75250 Paris Cedex 05, France

<sup>e</sup>Service d'Endocrinologie, Hôpital Avicenne, 125 rue de Stalingrad, 93009 Bobigny cedex, France

**Running title:** Type-II'  $\beta$ -turn CD and Raman markers

♦Contributed equally to the present work

\*Corresponding author ([mahmoud.ghomi@univ-paris13.fr](mailto:mahmoud.ghomi@univ-paris13.fr))

**Abbreviations.** SST-14, somatostatin-14; SSTR, somatostatin receptor; TSH, thyroid-stimulating hormone; c, cyclic; MeOH, methanol; TFA, trifluoroacetate; TFE, Tetrafluoroethylene; DMSO, dimethyl sulfoxide; Fmoc, 9-fluorenylmethyloxycarbonyl; tBu, tert butyl; HMBA, 4-(hydroxymethyl) benzoic acid; AcM, acetamidomethyl; SPPS, solid phase peptide synthesis; Boc, t-butyloxycarbonyl; HATU, 2-(1H-7-Azabenzotriazol-1-yl)-1,1,3,3-tetramethyluronium hexafluorophosphate; DIPEA, N,N-diisopropylethylamine; DMF, dimethylformamide; CD, circular dichroism; NMR, nuclear magnetic resonance; RP-HPLC, reversed phase high performance liquid chromatography; TOF, time of flight; API, atmospheric pressure ionization; ES-MS, electro spray mass spectroscopy.

## Abstract

Octreotide, a potent somatostatin analogue, is used as an antiproliferative drug in numerous endocrine tumors. Previous NMR investigations, basically performed in DMSO, had evidenced a type-II'  $\beta$ -turn structure for this cyclic peptide. However, apart a few incomplete studies by circular dichroism, a systematic analysis of the structural behavior of octreotide in aqueous solution as a function of concentration and ionic strength was still lacking. Here, we report the chemical synthesis and purification of octreotide for optical spectroscopic purposes accompanied by its structural analysis. Furthermore, we have used octreotide as a short size, well defined model compound for analyzing the CD and Raman markers of a type-II'  $\beta$ -turn. CD data collected in the 25-250  $\mu$ M range revealed the general trend of octreotide to undergo a disordered toward ordered structural transition upon increasing concentration. Especially, the  $\beta$ -turn CD markers could be characterized above 50  $\mu$ M, by a negative band at  $\sim$ 202 nm flanked by a shoulder at  $\sim$ 218 nm. On the basis of Raman spectra recorded as a function of concentration (1-20 mM), we could assign the markers at  $\sim$ 1678 and  $\sim$ 1650  $\text{cm}^{-1}$  in the amide I region, and at  $\sim$ 1303,  $\sim$ 1288 and  $\sim$ 1251  $\text{cm}^{-1}$  in the amide III region, to the type-II'  $\beta$ -turn structure. The stability of the intermolecular anti-parallel  $\beta$ -sheet formed in octreotide could be confirmed by the rigidity of the disulfide bridge which adopts a preferential *gauche-gauche-gauche* rotamer along the  $-\text{C}\beta\text{-S-S-C}\beta-$  moiety of the linked cysteines. The present analysis permits a better understanding of the differences between the structural features of SST-14 and its routinely used analogue, octreotide.

**Keywords:** Octreotide, Somatostatin-14, Circular dichroism, Raman scattering

## Introduction

Octreotide, *FCFWKTCT*(ol), where italic letters correspond to D-type isomers, is a cyclic octapeptide with a disulfide bridge between the two cysteines at its 2 and 7 positions. First synthesized in 1980,<sup>1</sup> this octapeptide is considered as a potent and selective analogue of the natural cyclic hormone SST-14.<sup>2,3</sup> The latter peptide is produced by neuroendocrine neurons of the hypothalamus and carried to the anterior pituitary gland, where it inhibits the secretion of growth hormone from somatotrope cells. SST-14 is also widely distributed throughout all the central nervous system, the gastrointestinal tract and the pancreas. Through binding to five specific cell surface receptors (SSTR<sub>i</sub>, *i*=1,...,5) it exerts a variety of physiological effects, and has obviously a broad therapeutic potential.<sup>4</sup> Unfortunately, SST-14 has a very short plasma half-life (<2 min), which is a major hindrance for an actual therapeutic goal. In this framework, octreotide with its special chemical composition, has shown an increased biological efficiency in inhibiting secretion of growth hormone, gastrin, glucagon, thyrotropin and insulin. Thanks to its multi-faceted pharmacologic profile, octreotide (Sandostatin®, Novartis Pharmaceuticals) provides broad therapeutic opportunities for several well-established indications such as Acromegaly, Gastrinoma, Pancreatitis, TSH-secreting pituitary adenomas, Diabetes, but also Carcinoid tumors.<sup>5-13</sup> Octreotide is now considered as standard of care for patients with newly diagnosed well-differentiated metastatic midgut tumors.<sup>14</sup>

As far as the octreotide structural features are concerned, its crystal data were published in 1995, revealing three molecules in the asymmetric unit (referred to as I, II and III), surrounded with water molecules.<sup>15</sup> All these molecules present a type-II'  $\beta$ -turn structure formed around D-Trp-Lys central residues. While molecule I has a regular flat anti-parallel  $\beta$ -sheet structure, the other two molecules present a distortion at their C-terminal part, favoring H-bonding with surrounding water molecules. Consistent with the crystal data, the detailed <sup>1</sup>H-NMR data collected in DMSO-d<sub>6</sub> were published two years later,<sup>16</sup> revealing two major

conformers, both folded through a type-II'  $\beta$ -turn. The relative population of these conformers has never been discussed. Although other NMR data obtained in a water/MeOH mixture had confirmed a similar  $\beta$ -turn structure for octreotide,<sup>17</sup> a complete structural analysis of this SST-14 analogue in aqueous solution as a function of concentration and ionic strength was still lacking. Thus, we found that it is necessary to propose the present study in order to answer to some not yet elucidated aspects. We have previously shown that an experimental protocol based on the joint use of CD and Raman spectra permits a suitable analysis of the structural and dynamical properties of the short peptides in aqueous media.<sup>18-21</sup> Another interesting aspect of the present report is that octreotide can be considered as a simple model compound for analyzing as accurately as possible the conformational markers of the type-II'  $\beta$ -turn by optical spectroscopy, taking account of the fact that equilibrated signals are expected from the turn and its stabilizing anti-parallel  $\beta$ -sheet.

It is a matter of fact that the relevance of the expected optical spectroscopy data highly depends on the quality of the peptide sample, namely the purity, solubility and knowledge of the exact concentration of the chemically synthesized octreotide. Besides fragment condensation solution-phase methods, suitable for commercial manufacture,<sup>22,23</sup> not-conventional solid phase processes have already been developed to synthesize this peptide on a smaller scale. Focusing on Fmoc/tBu strategies, several linkers are able to release upon standard cleavage peptide alcohols, such as tetrahydropyranyl<sup>24,25</sup> or chlorotriyl with either direct recovery of C-terminus alcohol function,<sup>26,27</sup> or after an O-N acyl migration additional step upon the deprotected isopeptide.<sup>28</sup> Otherwise, the reductive cleavage of an HMBA-type (4-hydroxymethyl benzoic acid) ester linkage with LiBH<sub>4</sub> or NaBH<sub>4</sub>/LiBr<sup>29</sup> is not compatible with on-resin disulfide bridge formation and therefore not advisable for octreotide SPPS. Alternatively, aminolysis with threoninol of D-Phe-c[Cys-Phe-D-Trp(Boc)-Lys(Boc)-Thr(tBu)-Cys]-HMP resin was shown to produce octreotide with a yield of 14%.<sup>30</sup> On-resin

intramolecular disulfide bond formation is usually performed from Ac<sup>m</sup>-protected thiols and by treatment with either I<sub>2</sub>, Hg(OAc)<sub>2</sub> or Tl(Tfa)<sub>3</sub> of the peptidyl-resin. Considering the over-oxidation eventuality associated with iodine-mediated oxidation, and the mercury-peptide adduct often observed after mercuric acetate treatment, Tl(Tfa)<sub>3</sub>, used as a milder oxidant, was shown to yield the best results, provided Trp residue was appropriately protected with the Boc group in order to avoid its modification.<sup>30</sup> In the present work, octreotide was synthesized stepwise from a commercially available preloaded O-t-Butylthreoninol 2-chlorotrityl resin,<sup>31</sup> followed by an on-resin oxidation procedure with thallium trifluoroacetate. Before thallium(III) oxidation, direct TFA-cleavage of a small amount of peptidyl-resin was carried out in order to estimate the synthesis yield associated to the linear sequence.

## Material and Methods

**Peptide Synthesis, Thallium Oxidation and Cleavage from the Resin.** The Synthesis of octreotide, D-Phe-Cys-Phe-D-Trp-Lys-Thr-Cys-Thr(ol), was carried out at a 100 μmoles scale from an O-t-Butylthreoninol 2-chlorotrityl resin, using the classical Fmoc/tBu methodology on an ABI 433 synthesizer (Applied Biosystems, Foster City, CA, USA) equipped with a conductivity flow cell to monitor Fmoc deprotection. Fmoc-amino acids were activated with HATU/DIPEA and single coupled with an eightfold molar excess with regard to the resin. At the end of the synthesis, the resulting peptidyl resin (1 eq.) was suspended in DMF/anisole (19:1). Disulfide bond formation was carried out on the resin by addition of Tl(III) trifluoroacetate (1.2 eq.). This suspension was gently stirred for 80 min at 0°C before extensive washing with DMF. Cleavage and side chains deprotection were accomplished in one step by treatment with 95:2.5:2.5 mixture of trifluoroacetic acid (TFA), triisopropylsilane (TIS) and water for 2 h at room temperature. After filtration of the resin, the cleavage mixture was poured into ice-cold diethyl ether. The peptide was isolated by centrifugation, washed

three times with diethyl ether, dried and solubilized in aqueous TFA before freeze-drying. Fmoc-Phe-OH, Fmoc-Lys(Boc)-OH, Fmoc-Thr(tBu)-OH, coupling reagents, N-methyl pyrrolidone (NMP) and TFA were purchased from Applied Biosystems. O-t-Butylthreoninol 2-chlorotrityl resin (capacity 0,81 mmol/g), Fmoc-Cys(Acm)-OH, Fmoc-D-Phe-OH and Fmoc-D-Trp(Boc)-OH were obtained from Merck-Novabiochem (Darmstadt, Germany). Piperidine, anisole, Tl(III) trifluoroacetate and TIS were purchased from Sigma-Aldrich (St Louis, MO, USA).

**HPLC Analysis and Purification.** Analysis of crude mixtures and purity control of the final peptide were performed by RP-HPLC on an Agilent (Santa Clara, CA, USA) 1100 Series liquid chromatograph and monitored with a photodiode array detector by absorbance at 230 nm, by applying a linear gradient of 20% to 30% of B (acetonitrile) in A (0.08% aqueous TFA, pH 2) over 20min at a 0.35ml/min flow rate on a Symmetry300 C18 3.5  $\mu$ m 2.1 $\times$ 100 mm column (Waters, Manchester, UK). The crude material was solubilized in a mixture of aqueous TFA and acetonitrile (20%) at a final concentration of 5 mg/ml and purified by RP-HPLC on a nucleosil 5 $\mu$ m C18 300 Å semi-preparative column, using a linear gradient (0,65%/min) of 22 to 35% acetonitrile in 0.08% aqueous TFA over 20 min at a 6 ml/min flow rate. The exact concentration of the purified Octreotide was determined by quantitative Amino Acid Analysis, giving an overall isolated peptide yield of 40% (to be compared with 74% peak area calculated from HPLC analysis of the crude).

**Electrospray Ionisation Mass Spectrometry.** Mass spectrometry was carried out on a quadrupole-TOF Micro mass spectrometer (Waters) equipped with a Z-spray API source and calibrated with a phosphoric acid calibration solution. Capillary, sample cone and extraction cone voltages were set at 3kV, 20V and 10V, respectively. Source and desolvation temperatures were set at 80 and 250°C, respectively. Data were acquired by scanning over the m/z range 150–2000 at a scan rate of 1 s and an interscan delay of 0.1 s. Crude and purified



peptides were dissolved in a mixture of water/methanol/acetic acid 49.5/49.5/1 v/v/v at a concentration of 1  $\mu\text{g}/\mu\text{l}$  and analyzed in positive-ion mode by infusion at a flow rate of 5  $\mu\text{l}/\text{min}$ . Two hundred spectra were combined and the resultant raw multicharged spectra were processed using the MaxEnt 3 deconvolution algorithm embedded in the Masslynx software.

**Sample Preparation.** Fresh pure water was obtained from a Millipore filtration system.  $\text{D}_2\text{O}$  (100% purity) was provided by Euriso-top (Saclay, France). Solutions were prepared by dissolving the lyophilized powder samples of octreotide in pure water containing or not 150 mM NaCl. Deuterated samples were prepared by dissolving the peptide directly in pure  $\text{D}_2\text{O}$ . Peptide stock solutions at 20 mM were prepared and diluted in order to reach lower concentrations. Generally, for each new sample obtained, the measurement was performed 24 h after its preparation, in order to achieve the conformational equilibrium. It should be noticed that at the highest concentration, i.e. 20 mM, with or without addition of NaCl, a foamy solution was initially obtained, showing the peptide aggregation in aqueous solution. After a few minutes, bubbles disappeared gradually, enabling us to record Raman spectra with a reasonable scattering background.

**Circular Dichroism.** Dichroic signals from peptide samples were analyzed on a JASCO J-810 spectrophotometer. Samples were placed in suprasil quartz cells with 1 mm path length. Each spectrum, recorded in the 190-300 nm region, corresponds to the average of 5 scans with a speed of 100 nm/min (5 minutes of accumulation). CD spectra were baseline corrected and the measured ellipticity for each sample was normalized and expressed in  $\text{deg cm}^2 \text{dmol}^{-1}$ .

**Raman Scattering.** Stokes Raman spectra were recorded at room temperature in a suprasil quartz cell (5 mm path length). Samples were excited by means of the 488 nm line of an  $\text{Ar}^+$  laser (Spectra Physics) with an exciting power at the sample of  $\sim 200$  mW. Scattered light at right angle was analyzed on a Jobin-Yvon T64000 in a single spectrograph configuration with a 1200 grooves/mm holographic grating and a holographic notch filter. A

liquid nitrogen cooled CCD detection system (Spectrum One, Jobin-Yvon) was used to collect Raman data. Effective spectral slit width was set to *ca.* 5 cm<sup>-1</sup>. Each spectrum corresponds to a total acquisition time of 1200 s. No large fluorescence background developed under laser light, assigned to the photodecomposition of the Trp residue, was observed in our experiments. The solution remained clear without any color change during the whole experiment.

**Post-record Treatment of CD and Raman spectra.** Buffer subtraction and smoothing of observed spectra were performed by GRAMS/32 software (Galactic Industries). TFA contribution to the amide I and III regions, was easily subtracted as previously described.<sup>16</sup> The analysis of amide I, amide III and disulfide bond-stretch regions of Raman spectra was performed by curve fitting by means of Gaussian+Lorentzian functions, with the Lorentzian contribution kept equal to, or greater than 50%. Final presentation of CD and Raman spectra was achieved by means of SigmaPlot package (Systat Software Inc., Point Richmond, CA).

## Results and discussion

**HPLC and ES-MS analyses.** The integrity of the linear Acm-thiol-protected peptide was assessed by analytical HPLC and electrospray mass spectrometry (Figure 1A) (observed mass 1163,5111; expected M+H<sup>+</sup> 1163,5376). The synthesis yield was estimated to 92% as calculated by integration of the major peak in the crude RP-HPLC profile, recorded by absorbance at 230 nm (Figure 2A). After a 80 minutes on-resin treatment with Tl(III) trifluoroacetate in DMF and consecutive TFA-cleavage, Acm-deprotection/cyclisation yield was estimated to 82% as observed by HPLC analysis of the crude in the same conditions (Figure 2B). After purification on a C18 semi-preparative column, octreotide was finally checked by HPLC (Figure 2C) and ES-MS (Figure 1B) (observed mass 1019,4562–expected

M+H<sup>+</sup> 1019,4477). Quantification of the total net peptide content gave an overall isolated peptide yield of 40%.

**CD markers for a type-II'  $\beta$ -turn.** The previously published CD spectrum of octreotide, recorded in water at ~200  $\mu$ M, revealed a negative band peaking at ~202 nm, followed by a large shoulder at ~218 nm.<sup>32</sup> A similar shape has been observed at a lower concentration, i.e. 100  $\mu$ M.<sup>30</sup> In contrast, another report on the CD spectrum at 200  $\mu$ M recorded in methanol had shown a less pronounced shoulder around 217 nm.<sup>33</sup>

Here, we present a more complete concentration dependent scheme of CD spectra in aqueous solutions (Figure 3). In the 25-100  $\mu$ M range in pure water (Figure 3A), a redshift (199  $\rightarrow$  202 nm) of the deepest minimum is observed along with a blueshift (220 $\rightarrow$ 218 nm) of the negative shoulder. Except a general decrease of the positive CD signal above 230 nm, only small changes can be observed at lower wavenumbers, at the concentrations above 50  $\mu$ M (Figure 3A). These results permit a better understanding of the constancy of the previously reported CD spectra, all recorded above 100  $\mu$ M in water.<sup>31,32</sup> CD spectra in the presence of 150 mM NaCl (Figure 3B), also show a general decrease of the positive signal above 230 nm, with an additional surprising effect: the recorded signal resembles somehow the superposition of those observed below and above 50  $\mu$ M in pure water (Figure 3A); see for instance in Figure 3B, the two partially resolved negative peaks at 199 and 202 nm, as well as the enlarged shoulder in the 210-220 nm range.

Consequently, we can confirm that upon increasing concentration, a gradual conformational transition toward an ordered structure is observed (Figure 3A). This transition is altered by the salt content (Figure 3B), presumably through a charge screening by counter-ions, avoiding a complete conformational interconversion. Another effect induced by NaCl is a dramatic 2.5 fold decrease of CD intensity (from -1000 to -400 for the deepest minima). Previous studies on SST-14 could reveal the contribution of aromatic amino acids, especially

Phe, to the positive CD signal above 230 nm.<sup>34</sup> Thus, the CD hypochromism, observed with the concentration increase (Figures 3A and 3B), might be undoubtedly due to the peptide auto-association through a possible  $\pi$ -stacking of aromatic rings.<sup>35,36</sup>

**Raman markers for a type-II'  $\beta$ -turn.** It is worth noting that the minimum concentration needed for Raman spectroscopy (1 mM) is twice the maximum value used in CD spectroscopy. Thus, the auto-association effect, described in the preceding paragraph, should be much more important in the samples used for Raman spectra. Figure 4 compare these spectra obtained in H<sub>2</sub>O and D<sub>2</sub>O. Tentative assignment of the observed bands is based on our preliminary studies of the constituting amino acids, i.e. Lys,<sup>37</sup> Phe,<sup>38</sup> Trp,<sup>38</sup> Cys<sup>39</sup> and Thr.<sup>40</sup> The most intense Raman bands arise either from the aromatic residues, or from methylene and methyl groups involved in the side chains. As far as the peptide backbone is concerned, the so-called amide I (1700-1625 cm<sup>-1</sup>) and amide III (1325-1225 cm<sup>-1</sup>) regions, together with that corresponding to the disulfide bond stretch,  $\nu$ (S-S), i.e. 540-500 cm<sup>-1</sup>, bring a wealth of information concerning the global and local conformational properties of octreotide. The assignment of the amide III Raman bands has been confirmed by their overall vanishing in D<sub>2</sub>O (Figure 4B), because they mainly originate from the backbone N-H bending modes,  $\delta$ (NH). Amide I Raman bands, corresponding to the backbone  $\nu$ (C=O) vibrations coupled with the adjacent  $\delta$ (NH) vibrational motion, are recognized by a  $\sim 10$  cm<sup>-1</sup> downshift upon deuteration.

Figures 5A and 5B present the band decomposition of the amide I and amide III regions for the spectra observed at 5 mM. Table 1 reports the populations of different secondary structure elements ( $\beta$ -turn,  $\beta$ -strand and random) estimated in the amide I region. These results manifest a general decrease of random population accompanied by an increase of  $\beta$ -strand population, proving the  $\beta$ -hairpin structuring with concentration. The addition of 150 mM NaCl at the ultimate concentration (20 mM) does not change considerably the

populations of different secondary structures. Furthermore, we could also verify the correlation between the Raman markers observed in the amide I and amide III regions, by comparing the sum of the areas of the components obtained in both spectral regions (Table 2). On the basis of this comparison we can undoubtedly assign to (i) random chains the two components observed at 1692 (amide I) and 1265 (amide III)  $\text{cm}^{-1}$ ; (ii)  $\beta$ -strands the components at 1663 (amide I) and 1235 (amide III)  $\text{cm}^{-1}$ ; (iii)  $\beta$ -turn those located in the amide I region at 1678 and 1650  $\text{cm}^{-1}$ , together with the three components in the amide III region at 1302, 1288 and 1251  $\text{cm}^{-1}$ .

In Figure 6, we have reported the decomposition of the  $\nu(\text{S-S})$  region observed at the two extreme concentrations, i.e. 2.5 and 20 mM. Table 2 shows a prominent contribution of the *gauche-gauche-gauche* rotamer of the  $-\text{C}\beta\text{-S-S-C}\beta-$  moiety in the linked cysteines, whatever the peptide concentration. This population reaches 93% at 20 mM. The *gauche-gauche-trans* rotamer of this linkage fluctuates around 10%, in the whole range of concentration.

**Comparison with the previously reported structural data on the type-II'  $\beta$ -turns.**  $\beta$ -hairpins are known as stabilizing structural elements in protein chains, and serve as connecting units between ordered segments such as helices and  $\beta$ -sheets.<sup>41-43</sup> They are mostly composed by tight  $\beta$ -turns, allowing the peptide chain to fold onto itself through two residues, generally referred to as  $i+1$  and  $i+2$  residues. Among these  $\beta$ -turns, those of reverse character, i.e. the so-called type-I' and type-II' (also referred to as type-I and type-II mirror images), were recognized as the most occurring ones.<sup>44</sup> The particularity of these  $\beta$ -turn types is that the  $\varphi$  angle of the  $i+1$  residue is positive ( $\varphi_{i+1} \sim +60^\circ$ ), leading to a restricted choice of the amino acid that can be placed at this position.<sup>43</sup> Based on this fact, synthetic peptides have been developed in order to favor the formation of type-I' and type-II'  $\beta$ -turns.<sup>45-47</sup> For instance, a substantial work based on CD and NMR spectra could prove that the octapeptide with the generic sequence Boc-Leu-Val-Val-D-Pro-Xxx-Leu-Val-Val-OMe, can fold onto a

$\beta$ -turn at the central D-Pro-Xxx (i+1, i+2 residues, respectively). Interestingly, the presence of D-Ala or L-Ala at the position Xxx, favors either a stable type-I' or a type-II'  $\beta$ -turn, respectively.<sup>46</sup> CD signatures of these peptides observed in MeOH and TFE (solvents known for their higher structuring effect compared to water), could permit the assignment of a large negative band around 215 nm to the type-I'  $\beta$ -turn, whereas the type-II'  $\beta$ -turn was characterized by two partially resolved negative bands with the same intensities, around ~204 and ~218 nm.<sup>46</sup> No additional analysis in aqueous solution, especially as a function of concentration and ionic strength, was reported for these peptides.

We can thus assume that the tendency of octreotide to form a stable type-II'  $\beta$ -turn in aqueous solution is certainly due to the presence of the Trp residue at the i+1 position, probably reinforced by its D-isomer type, as well as to the existence of a disulfide bridge between its N<sup>ter</sup> and C<sup>ter</sup> cysteines. Considering the presently reported data, the CD signature observed for octreotide above 50  $\mu$ M (Figure 3A), with a double negative band at ~202 and ~218 nm, can be undoubtedly assigned to a type-II'  $\beta$ -turn. We should keep in mind that a weak contribution from the short intramolecular anti-parallel  $\beta$ -sheet to the shoulder at ~218 nm,<sup>48</sup> is possibly expected. Since the earliest interests for the vibrational markers of  $\beta$ -turns,<sup>49</sup> their assignments had still remained under discussion. Here, the Raman spectra of octreotide recorded for the first time, has offered us the opportunity to probe the amide I and amide III vibrational markers for a type-II'  $\beta$ -turn (Table 3 and Figure 5).

**Rigidity of the stabilizing intramolecular  $\beta$ -sheet.** This fact could be evidenced through the conformational flexibility of the disulfide bridge analyzed by Raman data. Previously, the molecular models constructed upon NMR data of octreotide,<sup>16</sup> revealed the existence of both *gauche-gauche-gauche* and *gauche-gauche-trans* rotamers around the -C $\beta$ -S-S-C $\beta$ - moiety. It is interesting to note that our presently Raman spectra permitted the estimation of the relative

population of these rotamers, proving that the *gauche-gauche-trans* conformer corresponds in fact to a minor structural population (Table 3).

**Can CD and Raman markers discriminate between the type-II and its reverse type-II'  $\beta$ -turns?** In fact, the type-II and type-II'  $\beta$ -turns differ one from another by the opposite signs of the  $\phi$  and  $\psi$  angles associated to the i+1 and i+2 residues.<sup>43</sup> It is interesting to note that the CD spectrum of a type-II  $\beta$ -turn is characterized by a completely positive band at  $\sim 200$  nm, followed by a long positive tail up to 240 nm.<sup>50</sup> In other words, type-II and type-II'  $\beta$ -turns, which are the mirror images of one respect to the other, give rise to somehow *reverse CD signals*.

As far as the vibrational markers of these turns are concerned, a previous investigation on the Raman spectra of c(VPGVG)<sub>3</sub> and poly(VPGVG), have evidenced that two major amide I bands at 1676 and 1652 cm<sup>-1</sup> might both be considered as the type-II  $\beta$ -turn markers.<sup>51</sup> Note that these wavenumbers are very close to those assigned here to a type-II'  $\beta$ -turn, i.e.  $\sim 1678$  and  $\sim 1650$  cm<sup>-1</sup> (Figure 5A, Table 1). Regarding the amide III Raman markers, the same study had assigned to the type-II  $\beta$ -turn, a strong and broad band centered 1250 cm<sup>-1</sup>, flanked by a higher wavenumber weak band at 1284 cm<sup>-1</sup>. These wavenumbers fall again very close to the two components (out of three), i.e. at 1251 and 1288 cm<sup>-1</sup>, that we assign here to the amide III vibrations of a type-II'  $\beta$ -turn (Figure 5B). Thus, the main question is to find other proofs, beyond those described above, for assigning the remaining component at  $\sim 1302$  cm<sup>-1</sup> (Figure 5B) that we have also assigned to the amide III vibrations in octreotide. A previous detailed analysis based on the observations by means of ultraviolet resonance Raman (UVR) spectra,<sup>52-53</sup> has permitted establishment of useful empirical relations between the amide III wavenumbers and the  $\psi$  angles of the  $\beta$ -turn i+1 and i+2 residues.<sup>54</sup> Particularly, these relations could predict two markers, one at  $\sim 1309$  cm<sup>-1</sup> (very close to that observed here at

$\sim 1303\text{ cm}^{-1}$ ), and the other at  $\sim 1223\text{ cm}^{-1}$  (underestimated compared to that observed here at  $\sim 1251\text{ cm}^{-1}$ ). It is worth mentioning that both of these predicted wavenumbers were calculated by means of standard values, i.e.  $\psi_{i+1}=-120^\circ$  and  $\psi_{i+2}=0^\circ$ , for a type-II'  $\beta$ -turn.<sup>43</sup> It should be also emphasized that the predicted wavenumbers for a type-II  $\beta$ -turn were  $\sim 1226$  and  $1223\text{ cm}^{-1}$ ,<sup>54</sup> related to the standard angles  $\psi_{i+1}=+120^\circ$  and  $\psi_{i+2}=0^\circ$ , respectively.<sup>43</sup> Furthermore, following the same empirical relations,<sup>54</sup> only a type-II'  $\beta$ -turn can give rise to an amide III marker above  $1300\text{ cm}^{-1}$ . As a consequence, on the basis of the Raman markers, the two types (II and II') of  $\beta$ -turns can only be discriminated on the basis of their amide III highest wavenumber component observed at  $\sim 1302\text{ cm}^{-1}$ .

## Conclusions

Recently, other studies based on the joint use of vibrational circular dichroism (VCD) data and *ab initio* calculations,<sup>55</sup> or CD and UVRR spectra,<sup>56</sup> have permitted collection of very useful information on the structural features of  $\beta$ -turns in peptides, upon analysis of their amide regions (I, II and III). Our presently applied protocol, based on the CD and Raman data collected from octreotide in aqueous solution, allowed us especillay to get insight into the structural markers of its type-II'  $\beta$ -turn. Thanks to these data, we can confirm that there exist interesting differences between SST-14, and its routinely used analogue octreotide, as concerns their structural flexibility. In fact, within the submilimolar concentration range, CD spectra had shown that a clear ordered structure can never be achieved by SST-14,<sup>21</sup> whereas octreotide seems to be ordered with a stable type-II'  $\beta$ -turn, at the concentrartions above  $50\text{ }\mu\text{M}$ . However, SST-14, becomes structured in the milimolar range.<sup>21</sup> Furthermore, octreotide presents a lower conformational flexibility around its disulfide bridge, correlated to the structural rigidity of its intramolecular  $\beta$ -sheet.<sup>57</sup> All these evidences lead us to suggest that the flexible structure of SST-14 may be responsible for its aptitude to bind quite equivalently



to its five receptors (SSTR<sub>i</sub>,  $i=1, \dots, 5$ ), presumably through an *induced fit* process, whereas octreotide, with a more rigid structure, was shown to have a pronounced affinity towards SSTR<sub>2</sub>, along with a mediate one versus SSTR<sub>3</sub> and SSTR<sub>5</sub>.<sup>58,59</sup>

## Acknowledgements

The authors would like to thank Dr. Fernando Pflüger for his remarkable contribution to elucidating the structural and vibrational features of the building blocks of peptides by means of quantum mechanical calculations, which were granted access to the HPC resources of CINES (Montpellier, France) under successive allocations (2007-2012) made by GENCI (*Grand Equipement National de Calcul Intensif*).

## References

1. Bauer, W.; Briner, U.; Doepfner, W.; Haller, R.; Huguenin, R.; Marbach, P.; Petcher, T.; Pless, J. *Life Sciences* **1980**, *31*, 1134-1140.
2. Brazeau, P.; Vale, W.; Burgus, R.; Ling, N.; Butcher, M.; Rivier, J.; Guillemin, R. *Science* **1973**, *179*, 77-79.
3. Burgus, R.; Ling, N.; Butcher, M.; Guillemin, R. *Proc. Natl. Acad. Sci. USA*. **1973**, *70*, 684-688.
4. Patel, Y.C. *Frontiers in Neuroendocrinology*, vol. 20, no. 3, 1999, 157–198.
5. Anthony, L.; Freda, P.U. *Curr. Med. Res. Opin.* **2009**, *25*, 2989-2999.
6. Yang, L.P.; Keating, G.M. *Drugs* **2010**, *70*, 1745-1769.
7. Falchetti, A.; Marini, F.; Brandi, M.L. Multiple Endocrine Neoplasia Type 1, Pagon RA, Bird TD, Dolan CR, Stephens K (Eds), GeneReviews [Internet]. Seattle (WA): University of Washington, Seattle; 1993-2005 Aug 31 [updated 2010 Mar 02].
8. Grozinsky-Glasberg, S.; Barak, D.; Fraenkel, M.; Walter, M.A.; Müller-Brand, J.; Eckstein, J.; Applebaum, L.; Shimon, I.; Gross, D.J. *Cancer* **2011**, *117*, 1377-1385.
9. Chan, J.A.; Kulke, M.H. *Curr. Treat. Options Oncol.* **2011**, *12*, 136-148.
10. Gardner-Roehnelt, N.M. *Clin. J. Oncol. Nurs.* **2012**, *16*, 56-64.
11. Li, J.; Wang, R.; Tang, C. *Curr. Pharm. Des.* **2011**, *17*, 1594-1601.

12. Takahashi, N.; Nagamine, M.; Fukuda, M.; Motomura, W.; Abiko, A.; Haneda, M.; Fujiya, M.; Ieko, M.; Kohgo, Y. *Case Report. Med.* **2011**, 381203.
13. Modan-Moses, D.; Koren, I.; Mazor-Aronovitch, K.; Pinhas-Hamiel, O.; Landau, H. *J. Clin. Endocrinol. Metab.* **2011**, 96, 2312-2317.
14. Rinke, A.; Müller, H. H.; Schade-Brittinger, C.; Klose, K. J.; Barth, P.; Wied, M.; Mayer, C.; Aminossadati, B.; Pape, U. F.; Bläker, M.; et al. *J. Clin. Oncol.* **2009**, 27, 4656-4663.
15. Pohl, E.; Heine, A.; Sheldrick, G. M.; Dauter, Z.; Wilson, K. S.; Kallen, J.; Huber W.; Pfäffli, P. J. *Acta Cryst.* **1995**, D51, 48-59.
16. Melacini, G.; Zhu, Q.; Goodman, M. *Biochemistry* **1997**, 36, 1233-1241.
17. Widmer, H.; Widmer, A.; Braunn, W. *J. Biomol. NMR* **1993**, 3, 307-324.
18. Hernández, B.; Boukhalfa-Heniche, F. Z.; Coïc, Y. M.; Seksek, O.; Ghomi, M. *Biopolymers* **2006**, 81, 8-19.
19. Guiffo Soh, G.; Hernández, B.; Coïc, Y. M.; Boukhalfa-Heniche, F. Z.; Ghomi, M. *J. Phys. Chem. B* **2007**, 111, 12563-12572.
20. Guiffo-Soh, G.; Hernández, B.; Coïc, Y. M.; Boukhalfa-Heniche, F. Z.; Fadda, G.; Ghomi, M. *J. Phys. Chem. B* **2008**, 112, 1282-1289.
21. Hernández, B.; Carelli, C.; Coïc, Y. M.; De Coninck, J.; Ghomi, M. *J. Phys. Chem. B* **2009**, 113, 12796-12803.
22. Bauer, W.; Pless, J., (Sandoz) *Eur. Pat. Appl.* 29579. *US Pat* 4395403, **1981** and **1983**.
23. Chaturvedi, N. C.; Beri, S.; Yeole, R. D.; De Souza, N. J. *US Pat* 6987167, **2006**.
24. Thompson, L. A., and Ellman, J. A. *Tetrahedron Letters* **1994**, 35, 9333-9336.
25. Wu, Y. T., Hsieh, H. P., Chen, S. T., and Wang, K. T. *J. Chin. Chem. Soc.* **1999**, 46, 135-138.
26. Arano, Y.; Akizawa, H.; Uezono, T.; Akaji, K.; Ono, M.; Funakoshi, S.; Koizumi, M.; Yokoyama, A.; Kiso, Y.; Saji, H. *Bioconj. Chem.* **1997**, 8, 442-446.
27. Yim, C. B.; Boerman, O. C.; de Visser, M.; de Jong, M.; Dechesne, A. C.; Rijkers, D. T. S.; Liskamp, R. M. J. *Bioconj. Chem.*, **2009**, 20, 1323-1331.
28. Tailhades, J.; Gidel, M.A.; Grossi, B.; Lécaillon, J.; Brunel, L.; Subra, G.; Martinez, J.; Amblard, M. *Ang. Chem. Int. Ed.*, **2010**, 49, 117-120.
29. Stewart, J. M.; Morris, D. H. *Synthesis of peptide alcohols by the solid phase method, US patent* 4254023, **1981**.
30. Edwards, W. B.; Fields, C. G.; Anderson, C. J.; Pajean, T. S.; Welch, M. J.; Fields, G. *B. J. Med. Chem.* **1994**, 37, 3749-3757.

31. Morisco, A.; Accardo, A.; Gianolio, E.; Tesauro, D.; Benedetti, E.; Morelli, G. *J. Pep. Sc.* **2009**, *15*, 242-250.
32. Na, H. N.; Murty, S. B.; Lee, K. C.; Thanoo, B. C.; DeLuca, P. P. *AASP pharmSciTech* **2003**, *4*, 1-7.
33. Capone, S.; Kieltisch, I.; Flögel, O.; Lelais, G.; Togni, A.; Seebach, D. *Helv. Chim. Acta* **2008**, *91*, 2035-2056.
34. Holladay, L. A.; Rivier, J.; Puett, D. *Biochemistry* **1977**, *16*, 4895-4900.
35. Gazit, E. *FASEB* **2002**, *16*, 77-83.
36. Sal-Man, N.; Gerber, D.; Bloch, I.; Shai, Y. *J. Biol. Chem.* **2007**, *282*, 19753-19761.
37. Hernández, B.; Pflüger, F.; Derbel, N.; De Coninck, J.; Ghomi, M. *J. Phys. Chem. B* **2010**, *114*, 1077-1088.
38. Hernández, B.; Pflüger, F.; Adenier, A.; Kruglik, S. G.; Ghomi, M. *J. Phys. Chem. B* **2010**, *114*, 15319-15330.
39. Hernández, B.; Pflüger, F.; Adenier, A.; Kruglik, S. G.; Ghomi, M. *Phys. Chem. Chem. Phys.* **2011**, *13*, 17284-17294.
40. Hernández, B.; Pflüger, F.; Adenier, A.; Nsangou, M.; Kruglik, S. G.; Ghomi, M. *J. Chem. Phys.* **2011**, *135*, 055101.
41. Gunasekaran, K.; Ramakrishnan, C.; Balaram, P. *Prot. Eng.* **1997**, *10*, 1131-1141.
42. Santa, H.; Ylisirniö, M.; Hassinen, T.; Laatikainen, R.; Peräkylä, M. *Prot. Eng.* **2002**, *15*, 651-657.
43. Kaur, H.; Raghava, G. P. S. *Bioinformatics* **2004**, *20*, 2751-2758.
44. Sibanda, B. L.; Thornton, J. M. *Nature* **1985**, *316*, 170-174.
45. Richardson, J. S.; Richardson, D. C.; Tweedy, N. B.; Gernert, K.M.; Quinn, T. P.; Hecht, M. H.; Erickson, B. W.; Yan, Y.; McClain, R. D.; Donlan, M.E.; Surles, M. C. *Biophys. J.* **1992**, *63*, 1185-1209.
46. Das, C.; Naganagowda, G.A.; Karle, I.L.; Balaram P. *Biopolymers* **2001**, *58*, 335-346.
47. Rai, R.; Raghotama, S.; Sridharan, R.; Balaram, P. *Biopolymers* **2006**, *88*, 350-361.
48. Kelly, S. M.; Price, N. C. *Curr. Prot. Pep. Sc.* **2000**, *1*, 349-384.
49. Bandekar, J.; Krimm, S. *Proc. Natl. Acad. Sc. USA* **1979**, *76*, 774-777.
50. Perczel, A.; Fasman, G. D. *Prot. Sc.* **1992**, *1*, 378-395.
51. Thomas, G. J. Jr.; Prescott, B.; Urry, D. W. *Biopolymers* **1987**, *26*, 921-934.
52. Mikhonin, A. V.; Ahmed, Z.; Ianoul, A.; Asher, S. A. *J. Phys. Chem. B* **2004**, *108*, 19020-19028.

53. Ahmed, Z.; Beta I. A.; Mikhonin, A. V.; Asher, S. A. *J. Am. Chem. Soc.* **2005**, *127*, 10943-10950.
54. Mikhonin, A. V.; Bykov, S. V.; Myshakina, N. S.; Asher, S. A. *J. Phys. Chem. B* **2006**, *110*, 1928-1943.
55. Kim, J.; Kapitán, J.; Lakhani, A.; Bouř, P.; Keiderling, T. A. *Theor. Chem. Acc.* **2008**, *119*, 81-97.
56. Ahmed, Z.; Scaffidi, J. P.; Asher, S. A. *Biopolymers* **2008**, *91*, 52-60.
57. Grace, C.R.R.; Erchegeyi, J.; Samant, M.; Cescato, R.; Piccand, V.; Riek, R.; Reubi, J.C.; Rivier J.E. *J. Med. Chem.* **2008**, *51*, 2676-2681.
58. Weckbecker, G.; Lewis, I.; Albert, R.; Schmid, H. A.; Hoyer, D.; Bruns, C. *Nat. Rev. Drug Discovery* **2003**, *2*, 999–1017.
59. Pawlikowski, M.; Meleń-Mucha, G. *Curr. Opin. Pharmacol.* **2004**, *4*, 608–613.

**Table 1.** Determination of the different structural elements existing in aqueous solution of octreotide on the basis of the Raman bands in the amide I region

Concentration	1 mM	2.5 mM	5 mM	10 mM	20 mM	20 mM/ 150 mM NaCl	Secondary structures
<b>Amide I</b>							
Components							
1692	16	16	13	10	10	13	Random
1678	39	39	46	45	42	40	$\beta$ -turn
1663	22	23	23	28	33	34	$\beta$ -strand
1650	23	22	18	17	15	13	$\beta$ -turn
Sum of areas	100	100	100	100	100	100	

Different contributions (with a sum normalized to 100 for each sample) are estimated through band decomposition of the amide I region. Each contribution represents a normalized band area. Contributions correspond in fact to average values within an accuracy of  $\pm 5$  for each of them.

\*See Figure 5A for band decomposition.

**Table 2.** Contribution of different secondary structure elements obtained from amide I and amide III regions

Concentration	Region	Random <sup>a</sup>	$\beta$ -turn <sup>b</sup>	$\beta$ -strand <sup>c</sup>	Sum
1 mM	amide I	16	62	22	100
	amide III	13	67	20	100
2.5 mM	amide I	16	61	23	100
	amide III	14	66	20	100
5 mM*	amide I	13	64	23	100
	amide III	14	66	20	100
10 mM	amide I	10	62	28	100
	amide III	10	67	20	100
20 mM	amide I	10	62	28	100
	amide III	10	65	25	100

Different contributions (with a sum normalized to 100 for each sample), are determined through band decomposition of the amide I and amide III regions.

<sup>a</sup>Estimated by the areas of the component at 1692  $\text{cm}^{-1}$  (amide I), or at 1265  $\text{cm}^{-1}$  (amide III). <sup>b</sup>Estimated by the sum of the areas of the components at 1678 and 1650  $\text{cm}^{-1}$  (amide I), or of those at 1303, 1288 and 1251  $\text{cm}^{-1}$  (amide III). <sup>c</sup>Estimated by the area of the component at 1663  $\text{cm}^{-1}$  (amide I), or at 1235  $\text{cm}^{-1}$  (amide III).

\*See Figures 5A and 5B for band decomposition.

**Table 3.** Disulfide bond conformation determined on the basis of Raman markers

Concentrations	2.5 mM*	5 mM	10 mM	20 mM*	-C $\beta$ -S-S-C $\beta$ - rotamer
Components					
506	87	89	89	93	gauche-gauche-gauche
520	13	11	11	7	gauche-gauche-trans
Sum of areas	100	100	100	100	

Different contributions (with a sum normalized to 100 for each sample), are determined by means of band decomposition of the disulfide bond stretch region. Each contribution represents a normalized band area. Contributions correspond in fact to average values within an accuracy of  $\pm 5$  for each of them.

\* See Figures 6A and 6B for band decomposition.

### Figure captions

**Figure 1.** MaxEnt 3 deconvoluted ESI-MS spectra of doubly AcM-protected crude peptide (A) and purified octreotide (B).

**Figure 2.** Analytical HPLC profiles of doubly AcM-protected crude peptide (A), crude (B) and purified (C) octreotide (Waters Symmetry 300 C18 3.5  $\mu$ m 2.1 x 100 mm column; 20–30% B in 20 min, 0.35 ml/min; A: 0.08% TFA aq; B: MeCN).

**Figure 3.** CD spectra of octreotide in pure water (A) and in the solutions containing 150 mM NaCl (B) observed at different concentrations.

**Figure 4.** Raman spectra obtained from the aqueous solutions of octreotide, recorded in H<sub>2</sub>O (A) and in D<sub>2</sub>O (B).

**Figure 5.** Focus on two characteristic spectral regions of the Raman spectra recorded at 5 mM in pure water. (A) amide I region, (B) amide III region. See also Tables 1 and 2 for details. The band decomposition of this spectral region is also presented. Observed spectrum is in red color and circles correspond to the sum of the calculated components.

**Figure 6.** Raman spectra of octreotide recorded in pure water at 20 mM (A) and 2.5 mM (B), in the disulfide bond stretch region. The band decomposition contains located at  $\sim 506$  and  $\sim 520$  cm<sup>-1</sup> assigned to the *gauche-gauche-gauche* and *gauche-gauche-trans* conformations of the S-S bridge, respectively. Observed spectrum is in red color and circles correspond to the sum of the calculated components. See also Table 3.

**Extra Figure for TOC.** Octreotide structure from NMR data, with an extra ribbon display of its type-II'  $\beta$ -turn, and a yellow color for its disulfide bridge.

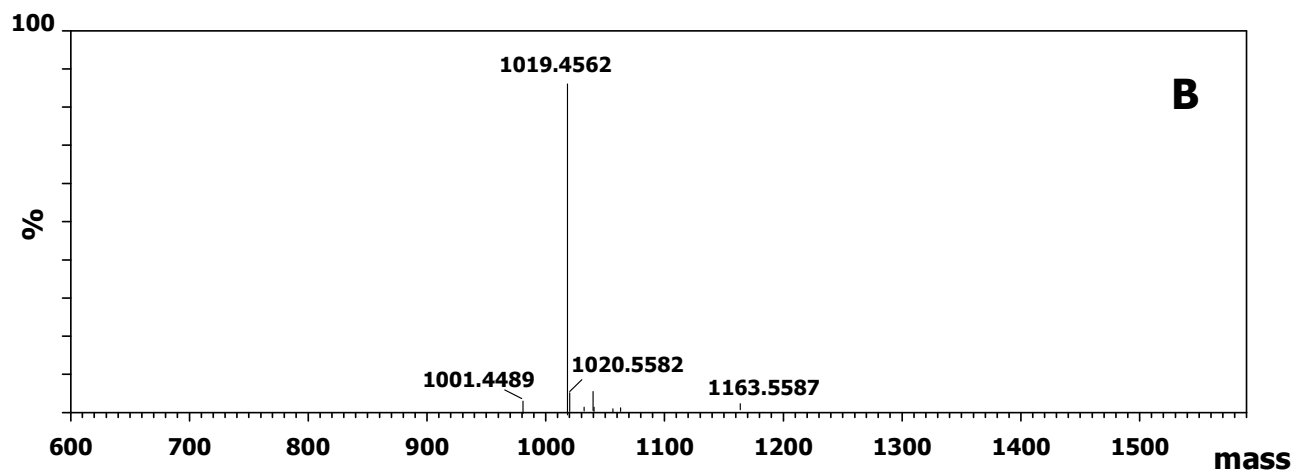
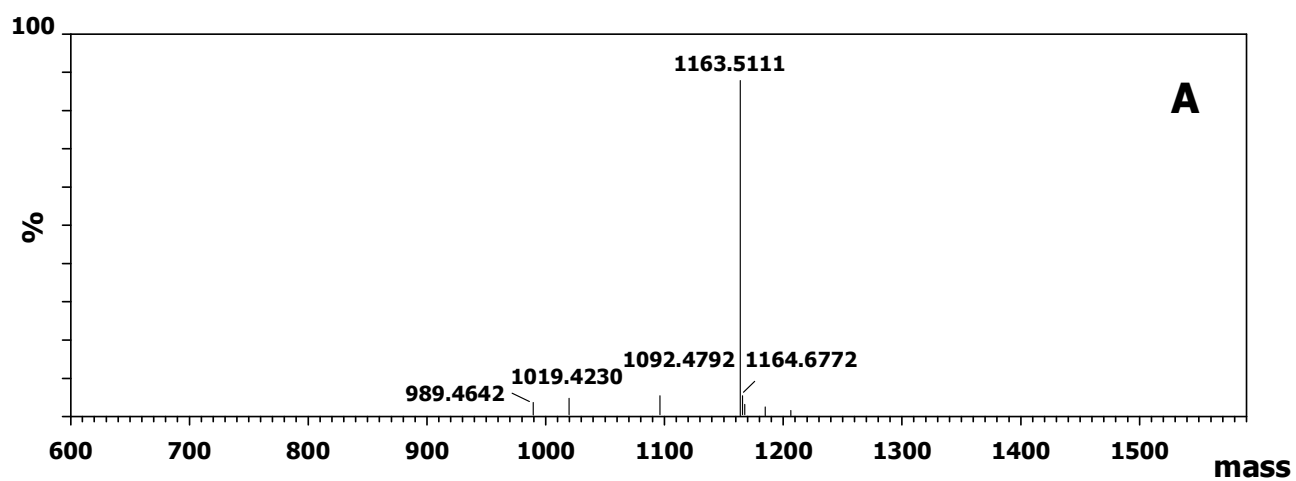


**Figure 1**

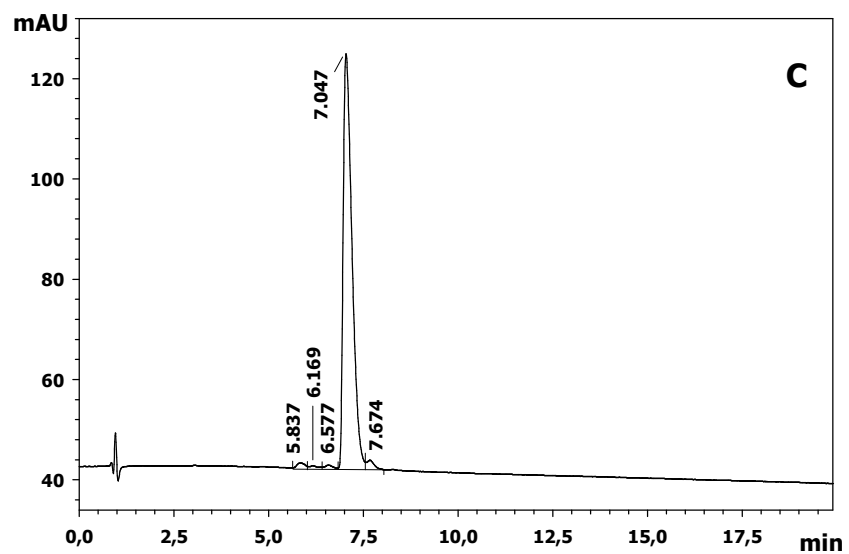
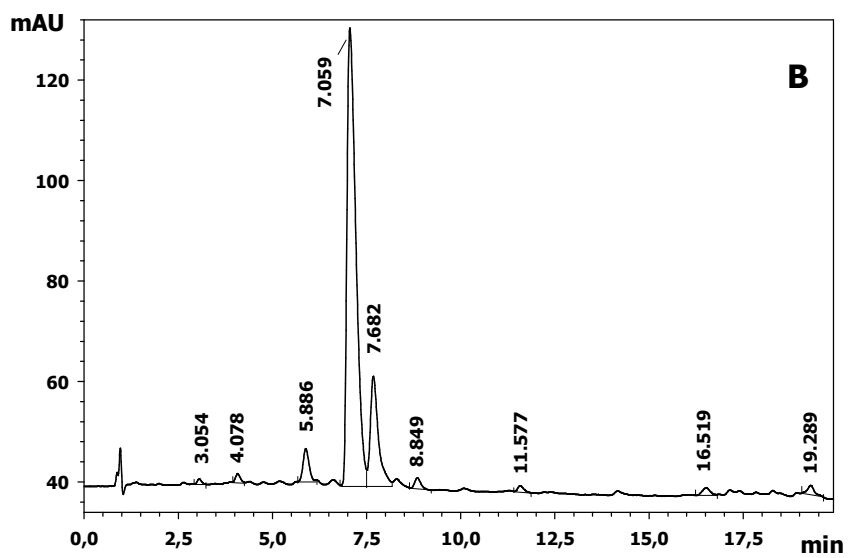
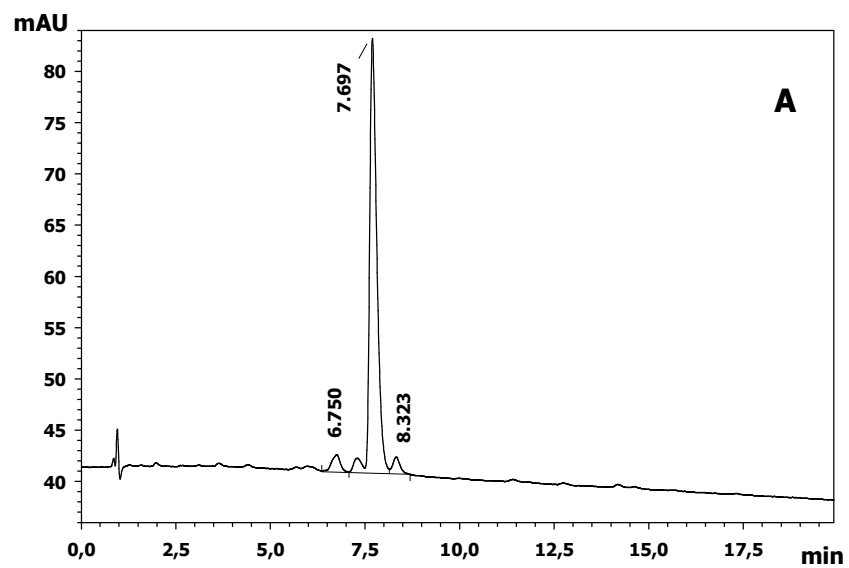


Figure 2



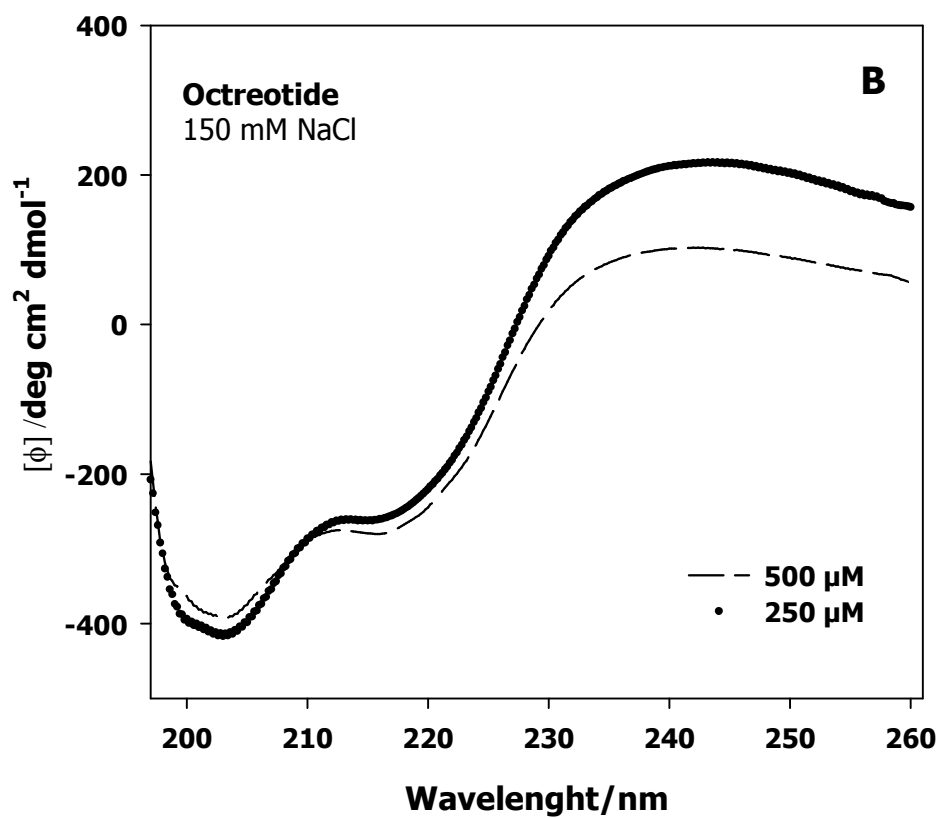
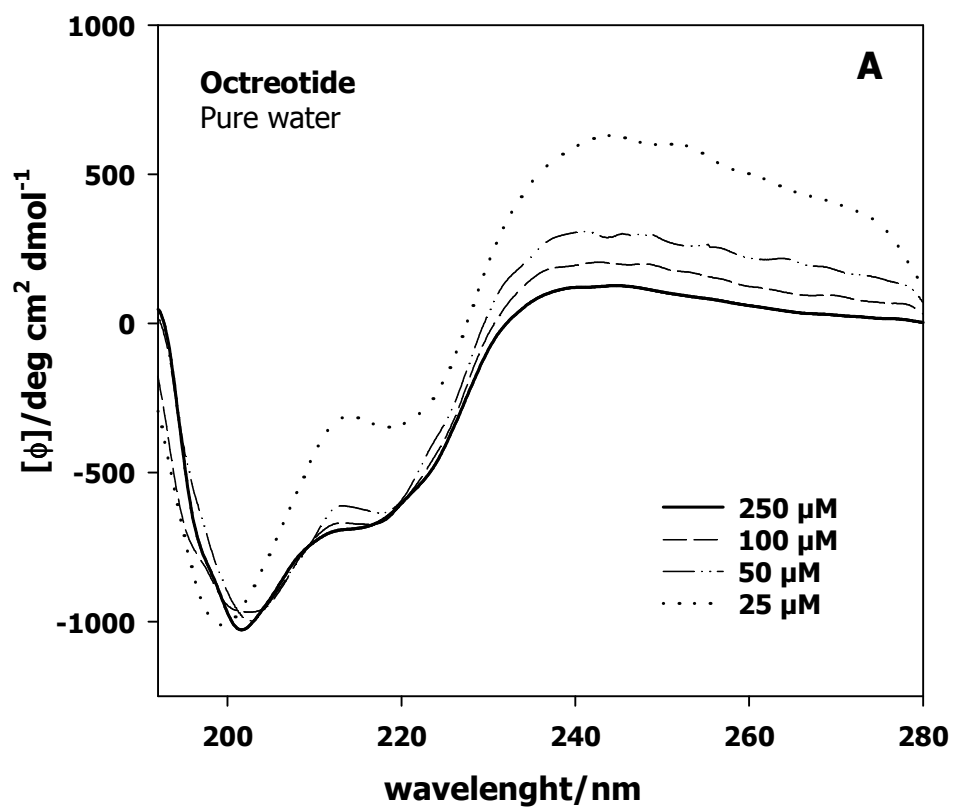
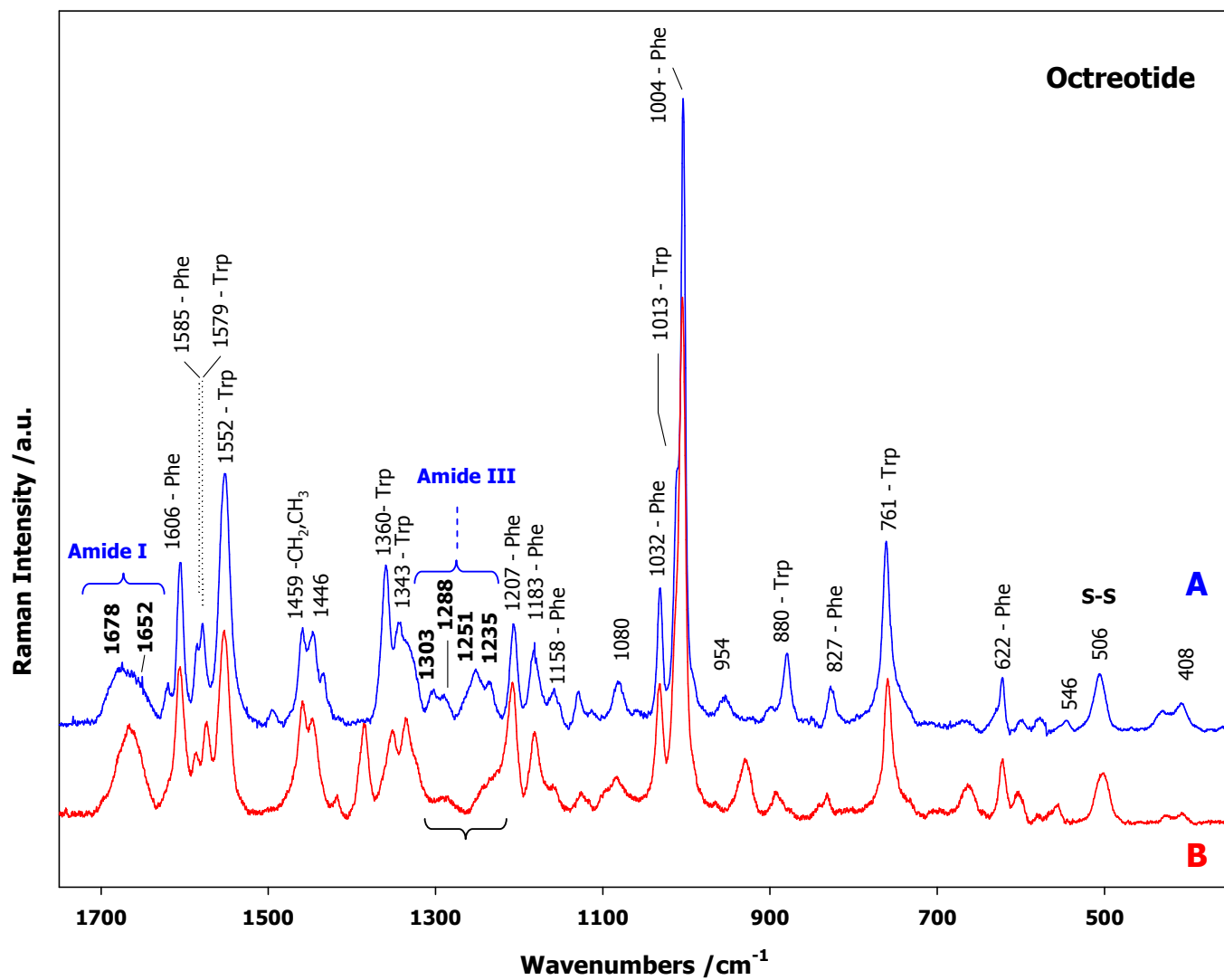


Figure 3



**Figure 4**

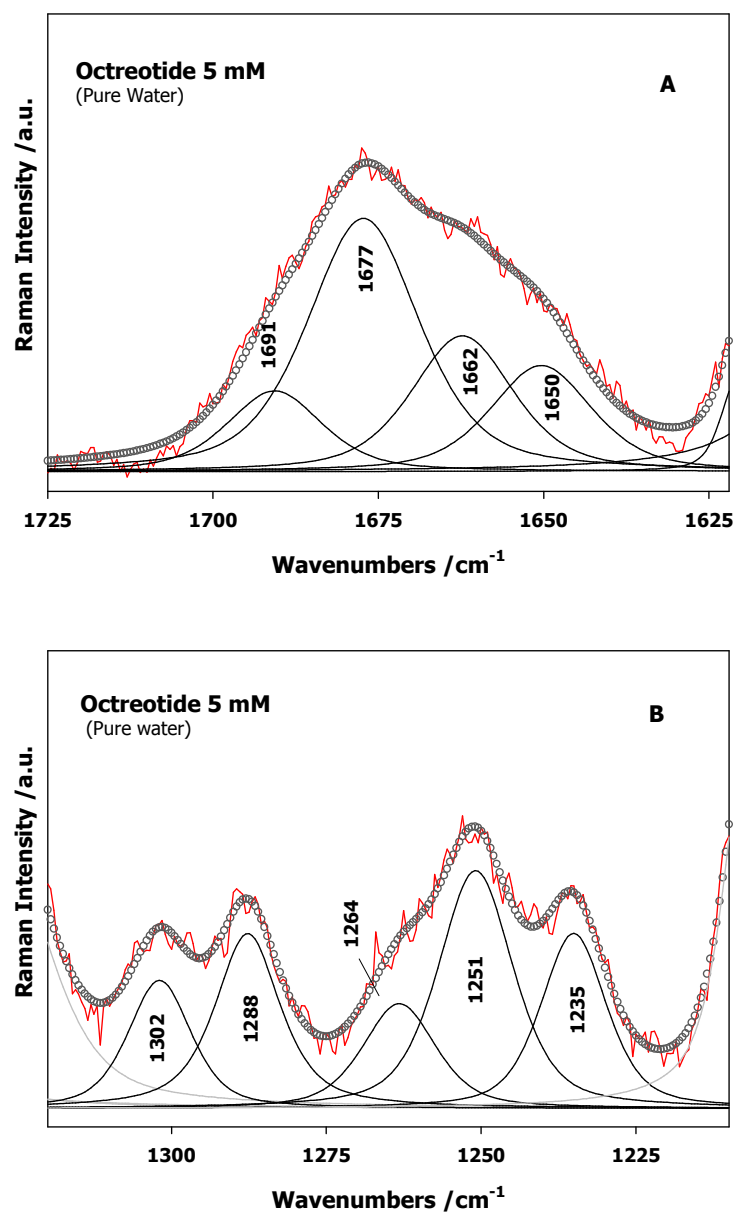


Figure 5

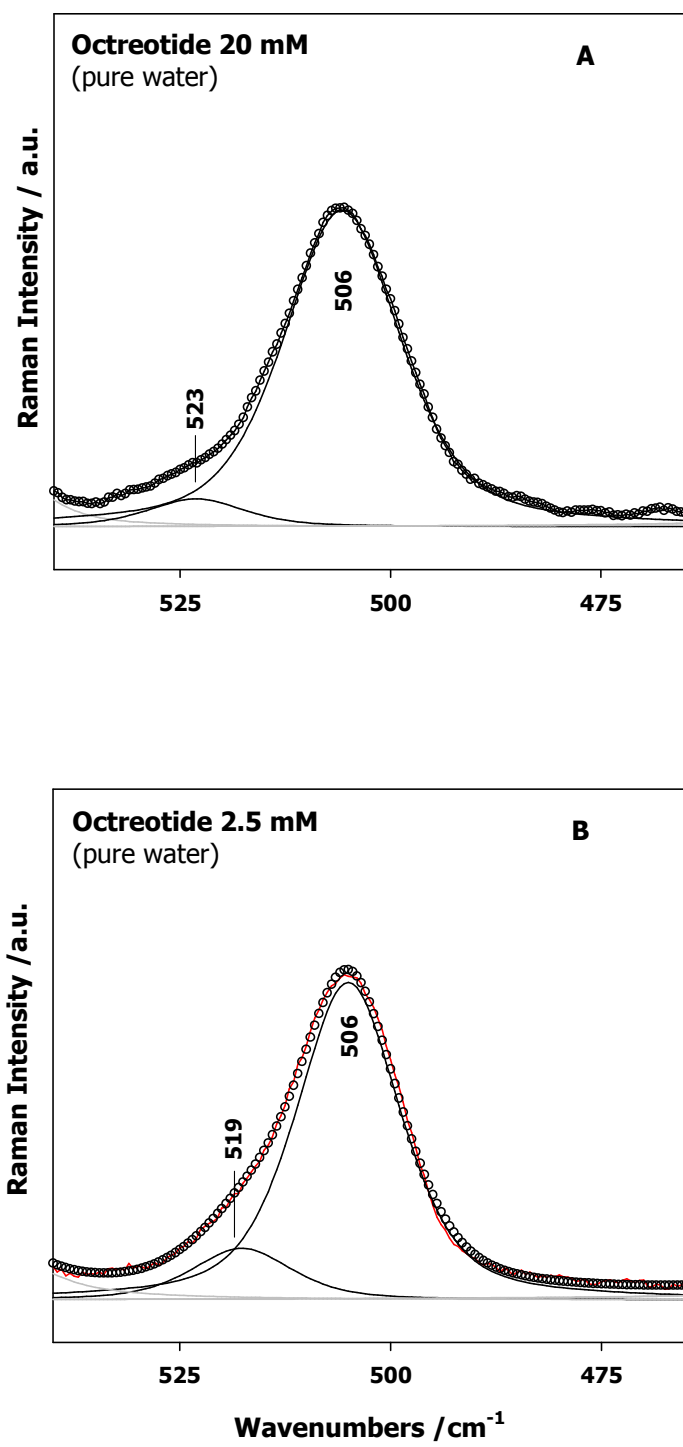


Figure 6

Extra Figure For TOC

